Journal of Bionic Engineering

Subject-specific Finite Element Modelling of the Human Shoulder Complex Part 1: Model Construction and Quasi-Static Abduction Simulation

--Manuscript Draft--

Manuscript Number:	JBEN-D-20-00070R2
Full Title:	Subject-specific Finite Element Modelling of the Human Shoulder Complex Part 1: Model Construction and Quasi-Static Abduction Simulation
Article Type:	Research Paper
Funding Information:	National Natural Science Foundation of China (No. 51475202) — Dr Lei Ren National Natural Science Foundation of China (51675222) — Dr Lei Ren Biotechnology and Biological Sciences Research Council (BB/H002782/1) — Dr Lei Ren National Natural Science Foundation of China (No. 91848204) — Dr Lei Ren Fundamental Research Funds for the Central Universities (76190-31610006) — Dr. Manxu Zheng Natural Science Foundation of Guangdong Province (2020A1515011292) — Dr. Manxu Zheng
Abstract:	Human shoulder joints exhibit stable but highly active characteristics due to the large amount of soft tissue. Finite element (FE) modelling plays an important role in enhancing our understanding of the mechanism of shoulder disorders. However, the previous FE shoulder models largely neglected the three-dimensional (3D) volume of soft tissues and their sophisticated interactions with the skeletons. This study develops a 3D model of the rotator cuff and deltoid muscles and tendons. It also includes cartilage and, for the first time, main ligaments around the joint to provide a better computational representation of the delicate interaction of the soft tissues. This model has potential value for studying the force transfer mechanism and overall joint stability variation caused by 3D pathological changes of rotator cuff tendons. Motion analysis systems and magnetic resonance (MR) scans were used to collect shoulder movement and geometric data from a young healthy subject, respectively. Based on MR images, a FE model with detailed representations of the musculoskeletal components was constructed. A multi-body model and the measured motion data were utilised to estimate the loading and boundary conditions. Quasi-static FE analyses simulated four instants of the measured scapular abduction. Simultaneously determined glenohumeral motion, stress/strain distribution in soft tissues, contact area, and mean/peak contact pressure were found to increase monotonically from 0° to 30° of abduction. The results of muscle forces, bone-on-bone contact force, and superior-inferior movement of the humeral centre during motion were consistent with previous experimental and numerical results. It is concluded that the constructed FE shoulder model can accurately estimate the biomechanics in the investigated range of motion and may be further used for the comprehensive study of shoulder musculoskeletal disorders.
Corresponding Author:	Lei Ren, Ph.D. The University of Manchester UNITED KINGDOM
Corresponding Author Secondary Information:	
Corresponding Author's Institution:	The University of Manchester
Corresponding Author's Secondary Institution:	

First Author:	Manxu Zheng
First Author Secondary Information:	
Order of Authors:	Manxu Zheng
	Zhihui Qian
	Zhenmin Zou
	Chris Peach
	Mohammad Akrami
	Lei Ren
Order of Authors Secondary Information:	

Abstract

Human shoulder joints exhibit stable but highly active characteristics due to a large amount of soft tissue. Finite element (FE) modelling plays an important role in enhancing our understanding of the mechanism of shoulder disorders. However, the previous FE shoulder models largely neglected the three-dimensional (3D) volume of soft tissues and their sophisticated interactions with the skeletons. This study develops a 3D model of the rotator cuff and deltoid muscles and tendons. It also includes cartilage and, for the first time, main ligaments around the joint to provide a better computational representation of the delicate interaction of the soft tissues. This model has potential value for studying the force transfer mechanism and overall joint stability variation caused by 3D pathological changes of rotator cuff tendons. Motion analysis systems and magnetic resonance (MR) scans were used to collect shoulder movement and geometric data from a young healthy subject, respectively. Based on MR images, a FE model with detailed representations of the musculoskeletal components was constructed. A multi-body model and the measured motion data were utilised to estimate the loading and boundary conditions. Quasi-static FE analyses simulated four instants of the measured scapular abduction. Simultaneously determined glenohumeral motion, stress/strain distribution in soft tissues, contact area, and mean/peak contact pressure were found to increase monotonically from 0° to 30° of abduction. The results of muscle forces, bone-on-bone contact force, and superior-inferior movement of the humeral centre during motion were consistent with previous experimental and numerical results. It is concluded that the constructed FE shoulder model can accurately estimate the biomechanics in the investigated range of motion and may be further used for the comprehensive study of shoulder musculoskeletal disorders.

Keywords: shoulder complex; biomechanics; finite element; glenohumeral joint; subject-specific

1 Introduction

The glenohumeral (GH) joint is the most mobile joint in the body [1]. Its stability is maintained mainly by soft tissues, especially the rotator cuff muscles [2]. Anterior shoulder dislocation, rotator cuff tears, bone fracture, and osteoarthritis are common shoulder disorders. However, the evaluation and diagnosis of these disorders remain challenging [3]. A better understanding of internal biomechanical conditions, such as joint contact forces, pressures, and areas, and the stress distribution in the muscle tendons, could help study shoulder pathologies. To obtain these internal

biomechanical conditions, computational simulation seems to be the most profound solution due to the limitation in measuring techniques and ethical considerations in traditional biomechanical measurements [4].

Previous computational shoulder models can be roughly classified into two broad categories: multi-body models based on rigid-body dynamics and finite element (FE) models based on continuum mechanics [5]. Multi-body models are commonly used to estimate muscle forces in-vivo [6]. However, the major simplifications of multi-body models preclude the acquisition of sophisticated deformations and stress distributions [5]. In contrast, the FE method is believed to be a powerful tool to assess these internal loading conditions of the shoulder [7]. In the last two decades, many FE shoulder models have been constructed based on various geometric configurations, material properties, and loading and boundary conditions. Early FE models of the shoulder focused on the supraspinatus tendon by using simplified two-dimensional geometry [8, 9]. Recent advanced medical imaging techniques have enabled three-dimensional (3D) geometric representation of the shoulder components [10, 11]. A comparison of recent studies with earlier studies reveals an increasing trend in accuracy and complexity that has proven beneficial [8-10, 12-14]. Recent studies mostly involved modelling 3D geometry of the bone and/or certain part of soft tissues to simulate a cadaveric experiment and validate predictions accordingly [11, 12]. However, shoulder joint stability is an overall performance of each musculoskeletal component, and most previous computational shoulder musculoskeletal models fail to use 3D subject-specific tissue geometry to represent this comprehensiveness.. This also hinders the definition of physiological loading and boundary conditions, although a number of different loading and boundary conditions have been used [10, 13, 15].

Subject-specific musculoskeletal modelling that allows the inclusion of individual musculoskeletal anatomy and properties can be clinically useful. Recent studies have increasingly tended to construct integrated biomechanical models using subject-specific measurements in the foot and femur modelling [16, 17]. These studies succeeded in simulating the internal conditions and in advancing our understanding of the biomechanical function of the musculoskeletal system. Technically, subject-specific modelling can ensure individualised characteristics and allow reasonable integration of different modelling and measuring techniques. Therefore, subject-specific modelling can enable the transfer of the data from multi-body and FE modelling as well as the 3D motion measurements, as all data are from the same subject; thus, it is suitable for computational modelling of the shoulder.

This study aims to develop a valid approach to incorporate 3D rotator cuff tendons and their delicate interactions with the humeral head in a FE shoulder model to better represent the mobile yet stable nature of the glenohumeral joint

computationally. The FE model allows simultaneous determination of GH motion, bone-on-bone contact force (BOBF: defined as the actual forces across the articulating surfaces that include the effects of muscles and ligaments [18]) and contact area, mean and peak contact pressure, and location of the peak pressure of the GH joint as well as the stress distribution in the rotator cuff tendons. These results were validated against experimental and numerical results. Besides, sensitivity studies of the material property definitions of the muscles and ligaments were tested against the results of the BOBF and peak pressure on the glenoid cartilage.

2 Materials and methods

2.1 Finite Element Modelling

The right shoulder of one healthy young male subject (age, 26 years old; height, 172 cm; weight, 66 kg) with no chronic or acute pain or injury was used through the whole study. The experiment was approved by Manchester University's Institutional Review Board, and the subject filled out the informed consent before the experiment. The geometric data were acquired using a 3.0T magnetic resonance imaging (MRI) scanner (Achieva, Philips Medical System, The Netherlands) when the subject was in the supine position with the arm in neutral rotation and adducted (thumbs-up) position. To facilitate the reconstruction, two sequences were performed: (1) T1-weighted axial scanning of the upper right body for the coverage of the whole right shoulder girdle (1.4 mm thick, 0.7-mm slice gap) and (2) proton density sagittal oblique scanning of the GH joint for the detailed tissue recognition (0.82 mm thick, 0.41-mm slice gap). The scanned images from both sequences were imported into Mimics software (Materialise NV, Leuven, Belgium), where most of the bones, muscles, tendons, ligaments, and cartilages were reconstructed geometrically. These reconstructed geometries were further constructed in SolidWorks (Dassault Systèmes, Waltham, MA, USA) for 3D solid-model generation. The humeral and the glenoid cartilages of the GH joint were considered as a thin layer lying on the subchondral bone defined as a uniform thickness of 0.6 mm and 1 mm (derived from the MR images), respectively [19]. A total of 13 tissue structures were constructed, including three bones: scapula, humerus, and clavicle; two cartilages: humeral and glenoid cartilage; four rotator cuff muscles: supraspinatus, infraspinatus, subscapularis, and teres minor; four ligaments: coracohumeral ligament, superior glenohumeral ligament, middle glenohumeral ligament, and inferior glenohumeral ligament. Finally, these 3D solid structures were imported, assembled, and meshed with 3D quadratic tetrahedral elements in Abaqus (v6.13 Simulia, Dassault Systèmes, USA). The total element number was 666,587 (see Fig. 1). A mesh convergence study showed that decreasing the element sizes of each component by half (increasing the element number to 2,758,946) improved the accuracy of the results of the BOBF and

peak pressure on the glenoid only by less than 5%. The material properties and element type used for modelling are listed in Table I. Tendon and muscles were considered as one musculotendon unit, accounting only for the passive behaviour [11]. As shown in Table I, the material property definition for most of the tissues involved was simplified as linear elastic followed previous studies. Since this study focus on the overall joint performance and force-transmitting mechanism evaluation, the chosen material properties definition is a compromise between accuracy and efficiency. The insertion and origin surfaces of the rotator cuff muscles were firmly attached to their relative bone surfaces at the proximal humerus and scapula. The contact between cartilages was defined as frictionless sliding. Similarly, the posterior rotator cuff tendons proximal to the insertion sites were defined to be frictionless sliding around the humeral head. Finally, the centre of the humeral head was determined as the centroid of a sphere fitted to the central part of the articular surface of the humeral head [20]. Also, the surface area of the glenoid cartilages (without labrum) was found to be 416 mm^2.

2.2 Scapular Abduction Measurement and Muscle Force Calculation

To obtain the physiological loading and boundary condition for the FE model, 3D motion capture, and muscle force prediction of the shoulder scapular abduction were conducted first (Fig. 2). For scapular abduction, arm elevation in the scapular plane was performed from neutral position to humerothoracic angle of 120° and adducted back, while keeping the elbow fully extended and the arm externally rotated (thumbs-up position) at a rate of approximately 5 seconds per cycle [21]. During measurement, the 3D locations of the reflective markers attached to each segment of the shoulder joint were determined using six infrared cameras of the 3D motion capture system (Vicon, Oxford, UK). Reflective markers were attached to the anatomical landmarks according to the recommendations of the International Society of Biomechanics (see Fig. S1, Fig. S2 and Table S1 in the supplement for details) [22]. In addition, one marker was attached to the middle point of the clavicle, one boomerang-shape acromion cluster with three markers was attached to the scapula on the flat portion of the acromion, and two rectangular clusters with four markers were attached to the humerus and forearm [23-25]. Before the abduction trials, a set of calibration procedures was used to locate the anatomical landmarks [25]. Marker trajectories were measured at a sampling frequency of 200 Hz and filtered by a fourth-order, zero-lag, low-pass Butterworth filter with a cut-off frequency of 3 Hz [26]. The scapular abduction trials were repeated 10 times to exclude random errors.

Subsequently, a generic 5-segment, 11-degrees-of-freedom multi-body musculoskeletal model of the upper limb was employed to calculate the muscle forces during scapular abduction in OpenSim [27, 28]. The 15 muscle bundles

around the GH joints represented rotator cuff, deltoid, pectoralis, latissimus dorsi, and coracobrachialis muscles. Markers on the model were placed following the markers' placement during 3D motion measurements (See section 2.2). Thereafter, mass and inertial properties, as well as the length of the segments and muscle-tendon bundles of this generic musculoskeletal model, were scaled to the subject's body measurements. Based on the motion data, the muscle forces were calculated by using the static optimisation in OpenSim [29]. It should be noted that only the magnitudes of these muscle forces were implemented in the following FE simulation. The directions of these forces in the FE simulation were determined by the reconstructed anatomy of the shoulder model. It was assumed that, for the same subject, the predicted muscle forces magnitudes in OpenSim simulation were equivalent to those in FE simulation.

2.3 Finite element simulation during scapular abduction

Quasi-static FE simulations of the shoulder at four instants of the measured motion, namely 0° (neutral), 10°, 20°, and 30° of abduction, were performed in Abaqus. Because the MRI data were obtained with the subject in a neutral adducted arm position, only the FE model in neutral was directly constructed. The geometric representations of the subject in the remaining abducted-arm positions were estimated based on the deformed geometries of all the components from the simulations conducted to reproduce the measured abduction motion to relative arm positions. Specifically, the deformed muscle geometries acquisition simulation were conducted by moving the humerus to the relative joint angle when fixing scapula [21]. During the rotation and translation, all rotator cuff muscles were manually pre-stressed to avoid compression occurring in any portion of the muscles and tendon. Thereafter, for each simulation, the scapula is considered as the fixed base reference segment, whereas the humerus is allowed to move [11, 12]. In this modelling configuration, the GH joint position and muscle forces obtained from the shoulder measurements can be applied, enabling investigation of the biomechanical functioning of the GH joint. Specifically, the clavicle and scapula were fixed, whereas the humerus was defined as free to move without any prescribed artificial control. Deltoid muscle forces and the rotator cuff muscle forces were implemented by extrinsic and intrinsic means, respectively. It was assumed that the applied muscle forces play a major role in the simulation shoulder movement. Extrinsically, the deltoid muscle forces (separated into anterior, middle, and posterior bundles) were directly applied by evenly distributed load acting on the insertion area and pointing to the centroid of their relative origin site (Fig. 3). Intrinsically, to mimic the muscle contraction, muscle forces of the rotator cuff muscles were applied through defining one-dimensional stress state (predefined tension) in the muscle belly portion in the initial condition. The direction of the one-dimensional stress state was set to be along the line connecting the centroids of the origin and insertion sites; the magnitude of the

one-dimensional stress was determined to reach the magnitude of muscle forces from OpenSim simulation. (The validation of the muscle forces implementation was conducted in separate muscle model that produced the same muscle forces as those from the multi-body simulation.) The GH motion, the stress/strain distribution on soft tissues, the GH contact state including the BOBF, contact area, pressure distribution, and peak pressure on glenoid were simultaneously determined in the simulation results. The position of the humeral centre in each abduction angle was calculated by refitting a sphere to the same central part of the articular surface of the humeral as mentioned earlier. The translation was determined by the changes in the humeral head centre between each joint angle.

2.4 Sensitivity analysis of material property

The sensitivity of BOBF and the peak pressure on the glenoid to the material property definitions of the muscles and ligaments were investigated in each abduction angle. Simulations were performed with varying ±5%, ±10%, ±20%, and ±40% of the elastic moduli of the muscles, ligaments, and cartilages, respectively.

3 Results

3.1 Muscle force calculation from OpenSim simulations

The muscle forces around the GH joints were calculated for 0° to 30° of scapular abduction. The predicted muscle forces of the rotator cuff muscles and the deltoid muscle bundles were found to be the largest among all of the calculated muscle forces in the OpenSim simulation. The magnitudes of muscle forces of these muscles at 0°, 10°, 20°, and 30° of scapular abduction can be found in Table II.

3.2 Quasi-static FE simulation results of the scapular abduction

With all muscle forces applied, quasi-static FE simulations were conducted at 0°, 10°, 20°, and 30° of abduction. The predicted Von Mises stress distribution on the soft tissues can be found in Fig. 4. (This study focuses on the modelling of the shoulder FE model. The Von Mises stress distribution is provided for demonstration purposes only. The choice of failure modes and results interpretation of the tissues should be made depending on the situation under investigation) Stresses on the rotator cuff muscles were found to be increasing over the volume with the increasing abduction angle. In each instant, relatively high-stress regions were found on the rotator cuff tendon section. Specifically, this high-stress region in the subscapularis tendon can be found around its osseous insertion, and this high-stress region

increased in stress magnitude and volume with the abduction monotonically. A similar trend was found in all posterior rotator cuff tendons. The detailed principal stress distribution in the supraspinatus tendon was plotted in slice views in the sagittal plane through the anterior, middle, and posterior section of the supraspinatus tendon at 30° abduction (see Fig. 5). It was found that, in the anterior section, the high stress was in the articular side of the tendon osseous insertion. In the middle section, the high stress was at the articular side where the supraspinatus wraps around the humeral head. In the posterior section, some portion of the infraspinatus tendon was included, and the high stress was found in the conjunction region of the supraspinatus and infraspinatus tendon from the articular to the bursal side.

In Fig. 6, the contact condition of the GH joint is highlighted in the penetrated view of the Von Mises stress distribution of the whole model, and this contact condition on the glenoid and humeral cartilages of each abduction angle are shown in the detailed joint-opened view. The variations of the contact pressure distribution, peak pressure, and position of the peak pressure on the glenoid during abduction are shown. Table III summaries these results with the simultaneous BOBF and superior-inferior movement of the humeral centre. The BOBF, GH contact area, and the mean and peak pressures on the glenoid were found to be increasing with the increasing abduction angle. Specifically, from 0° to 30° of abduction, BOBF, contact area, and the mean and peak pressure on the glenoid increased monotonically from 8.18 N to 408.07 N, 7.60 mm^2 to 88.04 mm^2, 1.07 MPa to 4.64 MPa, and 1.45 MPa to 7.66 MPa, respectively. The location of the peak contact pressure on the glenoid was found to be slightly above the centroid of the glenoid at 0° and 10° of abduction; at 20° of abduction it moved posteroinferiorly yet remained quite close to the centroid; however, it was found to move more posteriorly and eccentric from the centroid at 30° of abduction. Finally, in comparison to 0° of abduction, the superior-inferior movements of the humeral centre with respect to the glenoid at 10°, 20°, and 30° of abduction were found to be 1.43 mm, 2.08 mm, and 1.47 mm superiorly.

3.3 Sensitivity to material properties

The results of the variation of the BOBF and peak pressure on the glenoid due to the percentage

variation of modulus of muscle, cartilage and ligament material properties in each abduction angle are shown in Table IV and V. For most of the simulated results, the sensitivity decreased with the increasing of the abduction angle. The largest percentage variation is in 0° abduction when the muscle modulus decreased by 40%; as a result, the BOBF increased by 266.99% (from 8.18 N to 30.02 N), and the peak pressure increased by 116.55% (1.45 MPa to 3.14 MPa). For the remainder of the abduction angles, the largest percentage variations also occurred when the muscle modulus decreased by 40% (51.02%, 59.88%, and 20.47% in BOBF in 10°, 20°, and 30° of abduction, respectively). Comparing the sensitivity of different materials, the results were found to be highly sensitive to the variation of the muscle modulus, quite sensitive to the variation of the cartilage modulus, but only slightly sensitive to the variation of the ligaments (maximum increase by 12.71% when the modulus of ligament decreased by 40% for BOBF and 5.52% for peak pressure in ±40% of the modulus of the ligament). For muscle and ligament, the simulation results showed an almost negative linear response to the variation of elastic modulus of the respective soft tissues; i.e., the increase of the elastic modulus caused both results to decrease, and vice versa. In contrast, there was a positive linear response for cartilage variations.

4 Discussion

This study presents a FE model of a subject-specific shoulder joint by using an experimental-computational framework combining multi-body and FE modelling as well as 3D motion measurements. This FE model was created using 3D geometries of the major musculoskeletal components of the GH joint from high-resolution MR images. The model simplified ligament insertions representing them as discrete bands of connective tissue rather than a continuous sheet that blended with the joint capsule. In contrast, previous studies have either based on non-individualised data such as average anatomy [12], or focused only on a portion of a joint such as the supraspinatus tendon and humeral head [8, 9], ligaments and bones [10, 13], or labrum and glenoid [14]. Because the GH joint stabilising mechanism is believed to be an overall performance that requires effective functioning of

each part of the musculoskeletal structure [2], the comprehensiveness of the current model provides a basis for investigation of the mobility and stability nature of the GH joint as a whole.

In addition to the accurate 3D geometrical representation of the soft tissues, their delicate interactions with the humeral head were defined. The measured bone kinematics data were used in OpenSim simulation to inversely determine the dynamics of the model. The calculated muscle forces were applied in the FE simulation as the sole actuators to drive the model; Finally, the configuration of the loading and boundary condition of the FE model was set to accurately implement the data from the above two aspects: fixing scapula and clavicle, and applying muscle loads through muscle contractions and evenly distributed loads on the insertion site as described. In contrast, most previous studies used prescribed displacement of certain muscles and/or bones [13, 15], or cadaveric apparatus settings [10]. In this study, there were no prescribed artificial conditions for the humerus as commonly conducted in literature [8, 11, 12, 30, 31]. Instead, the humerus was actively positioned and stabilised by the calculated muscle loadings and passively by the surrounding tissue configurations. This definition allowed not only GH rotation but also translation, in contrast to the commonly defined ball-and-socket joint [32, 33]. It, therefore, reflected the stable yet mobile nature of the GH joint more realistically and enabled the determination of the GH contact state (Fig. 6) as well as the humeral movement (Fig. 8b). Furthermore, this feature (i.e., no artificial restriction) is particularly important for studying pathological conditions involving excessive humeral translation.

To evaluate the results, the predicted muscle forces were compared with three previous multi-body studies [26, 34, 35]. Among the results of the predicted muscle forces, the muscle force for teres minor and deltoid posterior proved to be quite small (maximum 6 N), in agreement with the results in the literature [34, 35]. The predicted muscle forces of the remainder of the muscles—namely, the deltoid anterior, deltoid middle, supraspinatus, infraspinatus, and subscapularis muscles—are illustrated with relevant literature data in Fig. 7. Despite some discrepancies, the general trend and magnitude of the predicted muscle forces demonstrated good agreement with previous literature. A significant difference

was found in the infraspinatus muscle, where relatively large forces were obtained. This probably comes from the relatively simple muscle bundle definition in the OpenSim model. Similar patterns found in infraspinatus muscle in a previous study that compared the influence of the number of muscle bundles and paths on the muscle force predictions [36].

Another important aspect worth discussing is the measurement noise. Noise mainly come from two sources which are the intrinsic noise from the measurement system and noise from experimental protocol [37]. The former noise can result from maker flickering, electronic noise and lens distortion. Since a high quality commercial optoelectronic stereophotogrammetric system was used in this study, it is assumed that these noises were acceptable. The latter noise, which the authors believe to be the main source of measurement error, is due mainly to the movement of the markers relative to the shoulder skeleton (skin artifacts) as well as from calibration uncertainties.

The results of the BOBF for each abduction angle were compared with the literature as shown in Fig. 8a [6, 34, 35, 38-40]. General good agreement of the magnitude and tendency was found. In particular, the BOBF of 0°, 10°, and 20° in this study were found to be almost the same as the in-vivo study [38], whereas the forces of 30° were found to be relatively large. Fig. 8b shows the comparison of superior-inferior movement of the humeral centre with respect to the glenoid during scapular abduction of three in-vivo kinematics studies [21, 41, 42]. Due to the difference between the measurement method and the definition of the coordinate system of GH joints, only the relative differences of the superior-inferior translations of between abduction angles were compared. In addition, the literature data which did not start from 0° abduction were adjusted to the equivalent results of this study. Specifically, the results of Bey et al. [41], (which started from 10° abduction) were set to start at 1.43 mm (the result of 10° of abduction in this study), and the results of Kijima et al. [42] (which started from 15° abduction) were set to start at 1.76 mm (the middle point of the results of 10° and 20° of abduction in this study) (see Fig. 8b). All the movement magnitude was provided in millimetres. The superior-inferior translation results of this study are in good agreement with the comparative results of the experimental

measurements. In particular, the initial superior movement of the humeral head to the point of 20° of abduction, followed by inferior movement in 30° of abduction from the results of Bey et al [41] were reproduced. This initial superior movement of the humeral head is consistent with the concept that the dynamic stabilisers (i.e., rotator cuff muscles) have not been fully activated in the early phase of abduction, due to gravity, the head position is superior to the starting position [21]. Later, with the start of the abduction, superior migration of the humeral head was observed [43, 44]. These comparisons indicated that the accuracy of the model is close to the previous study in predicating BOBF and at the same time quite accurate in predicating humeral translation with respect to the glenoid while few previous models had been able to describe this translation.

The magnitude of the BOBF comparison was found to be increasing monotonically in the abduction. This is reasonable, as more muscle forces were required to elevate the arm, which caused the increase of the BOBF to balance them. This result also demonstrated good agreement with previous numerical and experimental results (Fig. 8a). The determination of the BOBF in this study is a resultant of the contact state, which is a realistic reflection of the nature of the GH joint. In contrast, nearly all previous studies determined it the BOBF as the counterforce that restricted GH motion definition such as the ball-and-socket definition [6, 15, 34, 35, 39, 40].

The results of contact areas, mean and peak contact pressure, were found to be increasing from 0° to 30° of abduction. This increasing trend is logical, in that the BOBF is increasing with the abduction angle, which indicates that more compressive force is applied to the humeral head; hence the contact area with the glenoid fossa increased, which is consistent with previous studies [35, 45, 46]. Also, the location of the peak pressure in 30° of abduction was found in accordance with the previously reported measurements in both anterior-posterior and inferior-superior directions [47, 48]. The result of 88.04 mm^2 (which is 21.16% of the cartilage surface area of 416 mm^2) of the contact area in 30° of abduction in this study was compared with two in-vitro measurements; it was found consistent with one study of the average of 108 mm^2 (13.1% of the cartilage surface area) but less than the other study of 209 mm^2

(proportion of the cartilage surface area unknown) [46, 47]. The mean contact pressure of 4.63 MPa is close to the previously reported measurement of 4.35 MPa [47]. It should be noted that the labrum was not included in this study, which may have resulted in an underestimated contact area. Future work in this study will focus on integrating the labrum-biceps complex into the model to enable the model to investigate more complex shoulder biomechanical conditions.

Stresses on the rotator cuff muscles were found to be increasing over the volume with the increasing abduction angle. This result is reasonable because the muscle force increased and more loads were transferred from the muscles to the bones, which leads to this increase. Furthermore, the distribution of the maximum principal stress in the supraspinatus tendon of this study was plotted and compared with those from a previous study [11]. A similar stress state was found in the anterior and middle sections (Fig. 5 (a) and (b)). It should be noted that this study included some portions of the infraspinatus tendon, which was not modelled in the literature. Therefore, although similar high stress was found on the bursal side in both studies, the stress is actually within the infraspinatus tendon rather than the supraspinatus tendon (Fig. 5 (c)). This finding was also consistent with the anatomical study that reported the transverse part of the infraspinatus might be closely related to the supraspinatus at their insertions [49]. However, it should be noted that material properties definition differences might bring some uncertainty to this comparison.

The sensitivity study of the material properties demonstrated that the ligament definitions have little influence on the BOBF and peak pressure on the glenoid, whereas they were found to be sensitive to muscle and cartilage material property definitions. This may be due to ligaments loosening in the small abduction angles. The results of the BOBF and peak pressure on the glenoid cartilages were in linear response to the variation of Young's modulus of the muscle and cartilage. This is a reasonable result since the BOBF and peak pressure on the glenoid were generated as a result of the displacement of the humerus relative to the glenoid, which is the result of the variation of modulus of the muscle and cartilage. Also, 0° abduction is found to be the most sensitive to the variation of the material moduli

definition, probably because of the considerably small magnitude of the BOBF and peak pressure. The chosen mesh density is a good compromise between accuracy and efficiency. Based on the mentioned mesh convergence study in the method section, using relatively denser element sizes (ranged from 1.2 mm to 1.8 mm), the model demonstrated a relatively low discretisation error (5%) while keeping the computation economically acceptable (the model with half element sizes cost 99 hours for each simulation while the current model cost 40 minutes).

There are several limitations to this study. First, the complexity, which permitted the overall joint performance and force-transmitting mechanism evaluation, resulted in relatively large computational cost. Each FE simulation took 40 minutes to complete (24 cores). Second, the material property definition for most of the tissues involved was simplified as linear elastic, even though most of the soft tissues are a nonlinear, viscoelastic, inhomogeneous, and transversely isotropic material. Also, the major limitations of this study are that there was no differentiation between muscles and tendons, nor the simulation of the structure and orientation of the muscle fibres. It is worth mentioning that nonlinear muscle definitions have been used in previous studies [11, 31]. Moreover, recent advances in measuring techniques have enabled the in-vivo muscle material parameter determination [50]. These methods can be further used to improve the FE shoulder models in individualised material definitions. Third, it should be kept in mind that only a small range of motion was investigated in this study; this limits its application in explaining generic biological phenomena in larger ranges of motion. Finally, although most of the results were comparable to previous studies, direct validation was not performed. This omission was mainly attributable to technical limitations in direct measurement of the in-vivo conditions, such as the lack of direct in-vivo muscle loading and the GH joint contact measurement techniques in the biomechanics field. Future work is suggested to study the aforementioned aspects to obtain a more realistic shoulder FE model.

This study presents an important step towards our ultimate goal of quantifying in-vivo biomechanical state of the GH joint. This constructed model could find extensive applications. Firstly, the

simulation results in this paper revealed the contact mechanics and stress/strain distribution in soft tissues of the GH joint in the investigated range of motion, which provided the basis for the comparison of abnormal conditions. (Since the results obtained in this study are subject-dependent, the results may not be directly used for other studies.) The second part of this study showed the application of the model in investigating rotator cuff tears where simulation results were found to be consistent with the clinical observations and practices. Secondly, it has the potential to facilitate the development of pre-surgical planning and implant design/optimisation. Also, by implementing recent advanced discretisation techniques in real-time simulations [51-54], the model is possible to be used for real-time orthopaedic shoulder surgery simulations. Finally, the modelling techniques can be used for further FE modelling of the shoulder joint.

5 Conclusion

This study aims to develop a valid approach to include 3D rotator cuff tendons and their delicate interactions with the humeral head in a FE shoulder model to better represent the mobile yet stable nature of the glenohumeral joint computationally. The shoulder motion and geometric data of a young, healthy subject had been collected using a motion analysis system and MR scanning, respectively. A FE model with detailed representations of the musculoskeletal components was successfully constructed based on these MR images. Quasi-static FE analyses had been conducted to simulate four instants of the measured scapular abduction. Simultaneously determined GH motion, stress/strain distribution in soft tissues, contact area, and mean/peak contact pressure were found to increase monotonically from 0° to 30° of abduction. The results of muscle forces, bone-on-bone contact force, and superior-inferior movement of the humeral centre during motion were found to agree well with previous experimental and numerical results. These results revealed the internal biomechanical conditions of the GH joint in one healthy normal subject. It is concluded that the constructed FE shoulder model can accurately estimate the biomechanics in the investigated range of motion, which may be further used to compre-

hensively investigated shoulder musculoskeletal disorders. Further studies can be conducted based on the current model to further enhance our understanding of stabilising functions of the shoulder complex hence providing a theoretical basis for the evaluation and diagnosis of joint stability related shoulder musculoskeletal disorders.

Acknowledgements

This work was supported by the Grant of Biotechnology and Biological Sciences Research Council of GB (No. BB/H002782/1) and the Project of National Natural Science Foundation of China (No. 51475202 and No. 51675222).

We thank Ali Jabran, Kunyang Wang, Unene Gregory, and Dr Dan Hu for the motion capture measurement. We also thank Neal Sherratt and Prof. Waqar Bhatti for MRI scanning and reconstruction.

Conflict of Interest

The authors declare that the research was conducted in the absence of any commercial or financial relationships that could be construed as a potential conflict of interest.

References

[1]. Lippitt, S. and F. Matsen, Mechanisms of glenohumeral joint stability. ***Clinical Orthopaedics and Related Research***. 1993;291: 20-28.

[2]. Bigliani, L.U., R. Kelkar, E.L. Flatow, R.G. Pollock, and V.C. Mow, Glenohumeral stability: biomechanical properties of passive and active stabilizers. ***Clinical Orthopaedics and Related Research***. 1996;330: 13-30.

[3]. McFarland, E.G., J. Garzon-Muvdi, X. Jia, P. Desai, and S.A. Petersen, Clinical and diagnostic tests for shoulder disorders: a critical review. ***British Journal of Sports Medicine***. 2010;44(5): 328-332. DOI: 10.1136/bjsm.2009.067314.

[4]. Thibbotuwawa, N., Y. Gu, A. Oloyede, W. Senadeera, and T. Li. *Finite element shoulder models*. in ***Proceedings of 4th International Conference on Computational Methods (ICCM 2012)***. 2012. Gold Coast, Australia.

[5]. Zheng, M., Z. Zou, P.j.D.s. Bartolo, C. Peach, and L. Ren, Finite element models of the human shoulder complex: a review of their clinical implications and modelling techniques. ***International Journal for Numerical Methods in Biomedical Engineering***. 2016;33(2): e02777. DOI: 10.1002/cnm.2777.

[6]. Van der Helm, F.C., A finite-element musculoskeletal model of the shoulder mechanism. ***Journal of Biomechanics***. 1994;27(5): 551-569. DOI: 10.1016/0021-9290(94)90065-5.

[7]. Favre, P., J. Snedeker, and C. Gerber, Numerical modelling of the shoulder for clinical applications. ***Philosophical Transactions of the Royal Society of London A: Mathematical, Physical, and Engineering Sciences***. 2009;367(1895): 2095-2118. DOI: 10.1098/rsta.2008.0282.

[8]. Luo, Z.P., H.C. Hsu, J.J. Grabowski, B.F. Morrey, and K.N. An, Mechanical environment associated with rotator cuff tears. ***Journal of Shoulder and Elbow Surgery***. 1998;7(6): 616-620. DOI: 10.1016/S1058-2746(98)90010-6.

[9]. Wakabayashi, I., E. Itoi, H. Sano, Y. Shibuya, R. Sashi, H. Minagawa, and M. Kobayashi, Mechanical environment of the supraspinatus tendon: a two-dimensional finite element model analysis. ***Journal of Shoulder and Elbow Surgery***. 2003;12(6): 612-617. DOI: 10.1016/s1058274603002143.

[10]. Moore, S., B. Ellis, J. Weiss, P. McMahon, and R. Debski, The glenohumeral capsule should be evaluated as a sheet of fibrous tissue: a validated finite element model. ***Annals of Biomedical Engineering***. 2010;38(1): 66-76. DOI:

10.1007/s10439-009-9834-7.

[11]. Inoue, A., E. Chosa, K. Goto, and N. Tajima, Nonlinear stress analysis of the supraspinatus tendon using three-dimensional finite element analysis. ***Knee Surgery, Sports Traumatology, Arthroscopy***. 2013;21(5): 1151-1157. DOI: 10.1007/s00167-012-2008-4.

[12]. Walia, P., A. Miniaci, M.H. Jones, and S.D. Fening, Theoretical model of the effect of combined glenohumeral bone defects on anterior shoulder instability: a finite element approach. ***Journal of Orthopaedic Research***. 2013;31(4): 601-607. DOI: 10.1002/jor.22267.

[13]. Ellis, B., R. Debski, S. Moore, P. McMahon, and J. Weiss, Methodology and sensitivity studies for finite element modeling of the inferior glenohumeral ligament complex. ***Journal of Biomechanics***. 2007;40(3): 603-612. DOI: 10.1016/j.jbiomech.2006.01.024.

[14]. Yeh, M.-L., D. Lintner, and Z.-P. Luo, Stress distribution in the superior labrum during throwing motion. ***American Journal of Sports Medicine***. 2005;33(3): 395-401. DOI: 10.1177/0363546504268404.

[15]. Webb, J.D., S.S. Blemker, and S.L. Delp, 3D finite element models of shoulder muscles for computing lines of actions and moment arms. ***Computer Methods in Biomechanics and Biomedical Engineering***. 2012;17(8): 829-837. DOI: 10.1080/10255842.2012.719605.

[16]. Speirs, A.D., M.O. Heller, G.N. Duda, and W.R. Taylor, Physiologically based boundary conditions in finite element modelling. ***Journal of Biomechanics***. 2007;40(10): 2318-2323. DOI: 10.1016/j.jbiomech.2006.10.038.

[17]. Qian, Z.H., L. Ren, Y. Ding, J.R. Hutchinson, and L.Q. Ren, A Dynamic Finite Element Analysis of Human Foot Complex in the Sagittal Plane during Level Walking. ***Plos One***. 2013;8(11): e79424. DOI: 10.1371/journal.pone.0079424.

[18]. Winter, D.A., *Biomechanics and Motor Control of Human Movement*. 1987, Hoboken, New Jersey: University of Waterloo Press. 110-112.

[19]. Yeh, L., S. Kwak, Y.-S. Kim, D.S. Chou, C. Muhle, A. Skaf, D. Trudell, and D. Resnick, Evaluation of articular cartilage thickness of the humeral head and the glenoid fossa by MR arthrography: anatomic correlation in cadavers. ***Skeletal Radiology***. 1998;27(9): 500-504. DOI: 10.1007/s002560050427.

[20]. Graichen, H., T. Stammberger, H. Bonel, K.-H. Englmeier, M. Reiser, and F. Eckstein, Glenohumeral translation during active and passive elevation of the shoulder—a 3D open-MRI study. ***Journal of Biomechanics***. 2000;33(5): 609-613. DOI: 10.1016/S0021-9290(99)00209-2.

[21]. Matsuki, K., K.O. Matsuki, S. Yamaguchi, N. Ochiai, T. Sasho, H. Sugaya, T. Toyone, Y. Wada, K. Takahashi, and S.A. Banks, Dynamic in vivo glenohumeral kinematics during scapular plane abduction in healthy shoulders. ***Journal of Orthopaedic and Sports Physical Therapy***. 2012;42(2): 96-104. DOI: 10.2519/jospt.2012.3584.

[22]. Wu, G., F.C. van der Helm, H.E. Veeger, M. Makhsous, P. Van Roy, C. Anglin, J. Nagels, A.R. Karduna, K. McQuade, X. Wang, F.W. Werner, and B. Buchholz, ISB recommendation on definitions of joint coordinate systems of various joints for the reporting of human joint motion--Part II: shoulder, elbow, wrist and hand. ***Journal of Biomechanics***. 2005;38(5): 981-992. DOI: 10.1016/j.jbiomech.2004.05.042.

[23]. Ludewig, P.M., S.A. Behrens, S.M. Meyer, S.M. Spoden, and L.A. Wilson, Three-dimensional clavicular motion during arm elevation: reliability and descriptive data. ***Journal of Orthopaedic and Sports Physical Therapy***. 2004;34(3): 140-9. DOI: 10.2519/jospt.2004.34.3.140.

[24]. Warner, M.B., P.H. Chappell, and M.J. Stokes, Measuring scapular kinematics during arm lowering using the acromion marker cluster. ***Human Movement Science***. 2012;31(2): 386-96. DOI: 10.1016/j.humov.2011.07.004.

[25]. Ren, L., R.K. Jones, and D. Howard, Whole body inverse dynamics over a complete gait cycle based only on measured kinematics. ***Journal of Biomechanics***. 2008;41(12): 2750-2759. DOI: 10.1016/j.jbiomech.2008.06.001.

[26]. Yanagawa, T., C.J. Goodwin, K.B. Shelburne, J.E. Giphart, M.R. Torry, and M.G. Pandy, Contributions of the individual muscles of the shoulder to glenohumeral joint stability during abduction. ***Journal of Biomechanical Engineering***. 2008;130(2): 21-24. DOI: 10.1115/1.2903422.

[27]. Delp, S.L., F.C. Anderson, A.S. Arnold, P. Loan, A. Habib, C.T. John, E. Guendelman, and D.G. Thelen, OpenSim: open-source software to create and analyze dynamic simulations of movement. ***IEEE Transactions on Biomedical Engineering***. 2007;54(11): 1940-1950. DOI: 10.1109/TBME.2007.901024.

[28]. Holzbaur, K.R., W.M. Murray, and S.L. Delp, A model of the upper extremity for simulating musculoskeletal surgery and analyzing neuromuscular control. ***Annals of Biomedical Engineering***. 2005;33(6): 829-840. DOI: 10.1007/s10439-005-3320-7.

[29]. Erdemir, A., S. McLean, W. Herzog, and A.J. van den Bogert, Model-based estimation of muscle forces exerted during movements. ***Clinical Biomechanics***. 2007;22(2): 131-154. DOI: 10.1016/j.clinbiomech.2006.09.005.

[30]. Büchler, P., N. Ramaniraka, L. Rakotomanana, J. Iannotti, and A. Farron, A finite element model of the shoulder: application to the comparison of normal and osteoarthritic joints. ***Clinical Biomechanics***. 2002;17(9-10): 630-639. DOI: 10.1016/S0268-0033(02)00106-7.

[31]. Terrier, A., A. Reist, A. Vogel, and A. Farron, Effect of supraspinatus deficiency on humerus translation and glenohumeral contact force during abduction. ***Clinical Biomechanics***. 2007;22(6): 645-651. DOI: 10.1016/j.clinbiomech.2007.01.015.

[32]. Hopkins, A.R., U.N. Hansen, A.A. Amis, M. Taylor, N. Gronau, and C. Anglin, Finite element modelling of glenohumeral kinematics following total shoulder arthroplasty. ***Journal of Biomechanics***. 2006;39(13): 2476-83. DOI: 10.1016/j.jbiomech.2005.07.031.

[33]. Nikooyan, A.A., H.E.J. Veeger, E.K.J. Chadwick, M. Praagman, and F.C.T. van der Helm, Development of a comprehensive musculoskeletal model of the shoulder and elbow. ***Medical and Biological Engineering and Computing***. 2011;49(12): 1425-1435. DOI: 10.1007/s11517-011-0839-7.

[34]. Favre, P., M. Senteler, J. Hipp, S. Scherrer, C. Gerber, and J.G. Snedeker, An integrated model of active glenohumeral stability. ***Journal of Biomechanics***. 2012;45(13): 2248-2255. DOI: 10.1016/j.jbiomech.2012.06.010.

[35]. Sins, L., P. Tétreault, N. Hagemeister, and N. Nuño, Adaptation of the anybody™ musculoskeletal shoulder model to the nonconforming total shoulder arthroplasty context. ***Journal of Biomechanical Engineering***. 2015;137(10): 101006-101006. DOI: 10.1115/1.4031330.

[36]. Quental, C., J. Folgado, J. Ambrósio, and J. Monteiro, Critical analysis of musculoskeletal modelling complexity in multibody biomechanical models of the upper limb. ***Computer Methods in Biomechanics and Biomedical Engineering***. 2015;18(7): 749-759. DOI: 10.1080/10255842.2013.845879.

[37]. Della Croce, U. and A. Cappozzo, A spot check for estimating stereophotogrammetric errors. ***Medical and Biological Engineering and Computing***. 2000;38(3): 260-266.

[38]. Bergmann, G., F. Graichen, A. Bender, M. Kääb, A. Rohlmann, and P. Westerhoff, In vivo glenohumeral contact forces—measurements in the first patient 7 months postoperatively. ***Journal of Biomechanics***. 2007;40(10): 2139-2149. DOI: 10.1016/j.jbiomech.2006.10.037.

[39]. Poppen, N. and P. Walker, Forces at the glenohumeral joint in abduction. ***Clinical Orthopaedics and Related Research***. 1978;135: 165-170.

[40]. Terrier, A., A. Vogel, M. Capezzali, and A. Farron, An algorithm to allow humerus translation in the indeterminate problem of shoulder abduction. ***Medical Engineering and Physics***. 2008;30(6): 710-716. DOI: 10.1016/j.medengphy.2007.07.011.

[41]. Bey, M.J., S.K. Kline, R. Zauel, T.R. Lock, and P.A. Kolowich, Measuring dynamic in-vivo glenohumeral joint kinematics: technique and preliminary results. ***Journal of Biomechanics***. 2008;41(3): 711-714. DOI: 10.1016/j.jbiomech.2007.09.029.

[42]. Kijima, T., K. Matsuki, N. Ochiai, T. Yamaguchi, Y. Sasaki, E. Hashimoto, Y. Sasaki, H. Yamazaki, T. Kenmoku, and S. Yamaguchi, In vivo 3-dimensional analysis of scapular and glenohumeral kinematics: comparison of symptomatic or asymptomatic shoulders with rotator cuff tears and healthy shoulders. ***Journal of Shoulder and Elbow Surgery***. 2015;24(11): 1817-1826. DOI: 10.1016/j.jse.2015.06.003.

[43]. Ludewig, P.M. and T.M. Cook, Translations of the humerus in persons with shoulder impingement symptoms. ***Journal of Orthopaedic and Sports Physical Therapy***. 2002;32(6): 248-259. DOI: 10.2519/jospt.2002.32.6.248.

[44]. Deutsch, A., D.W. Altchek, E. Schwartz, J.C. Otis, and R.F. Warren, Radiologic measurement of superior displacement of the humeral head in the impingement syndrome. ***Journal of Shoulder and Elbow Surgery***. 1996;5(3): 186-193.

[45]. Hammond, G., J.E. Tibone, M.H. McGarry, B.-J. Jun, and T.Q. Lee, Biomechanical comparison of anatomic humeral head resurfacing and hemiarthroplasty in functional glenohumeral positions. ***Journal of Bone and Joint Surgery - American Volume***. 2012;94(1): 68-76. DOI: 10.2106/JBJS.I.00171.

[46]. Soslowsky, L., E. Flatow, L. Bigliani, R. Pawluk, G. Ateshian, and V. Mow, Quantitation of in situ contact areas at the glenohumeral joint: a biomechanical study. ***Journal of Orthopaedic Research***. 1992;10(4): 524-534.

[47]. Warner, J.J., M.K. Bowen, X.-h. Deng, J.A. Hannafin, S.P. Arnoczky, and R.F. Warren, Articular contact patterns of the normal glenohumeral joint. ***Journal of Shoulder and Elbow Surgery***. 1998;7(4): 381-388. DOI: 10.1016/S1058-2746(98)90027-1.

[48]. Yamamoto, A., D.F. Massimini, J. DiStefano, and L.D. Higgins, Glenohumeral contact pressure with simulated anterior labral and osseous defects in cadaveric shoulders before and after soft tissue repair. ***American Journal of Sports Medicine***. 2014;42(8): 1947-1954. DOI: 10.1177/0363546514531905.

[49]. Kato, A., A. Nimura, K. Yamaguchi, T. Mochizuki, H. Sugaya, and K. Akita, An anatomical study of the transverse part of the infraspinatus muscle that is closely related with the supraspinatus muscle. ***Surgical and Radiologic Anatomy***. 2012;34(3): 257. DOI: 10.1007/s00276-011-0872-0.

[50]. Clemen, C.B., G.E. Benderoth, A. Schmidt, F. Hübner, T.J. Vogl, and G. Silber, Human skeletal muscle behavior in vivo: Finite element implementation, experiment, and passive mechanical characterization. ***Journal of the Mechanical Behavior of Biomedical Materials***. 2017;65: 679-687. DOI: 10.1016/j.jmbbm.2016.09.030.

[51]. Bui, H.P., S. Tomar, and S.P.A. Bordas, Corotational Cut Finite Element Method for real-time surgical simulation: application to needle insertion simulation. ***Computer methods in applied mechanics and engineering***. 2019;345: 183-211. DOI: 10.1016/j.cma.2018.10.023.

[52]. Hadrien, C., A. Jérémie, K. Pierre, S.P.A. Bordas, C. Stéphane, and D. Christian, Real-time simulation of contact and cutting of heterogeneous soft-tissues. ***Medical Image Analysis***. 2014;18(2): 394-410.

[53]. Bui, H.P., S. Tomar, H. Courtecuisse, S. Cotin, and S.P.A. Bordas, Real-Time Error Control for Surgical Simulation. ***IEEE Transactions on Biomedical Engineering***. 2018;65(3): 596-607. DOI: 10.1109/tbme.2017.2695587.

[54]. Bui, H.P., S. Tomar, H. Courtecuisse, M. Audette, S. Cotin, and S.P.A. Bordas, Controlling the error on target motion through real-time mesh adaptation: Applications to deep brain stimulation. ***International Journal for Numerical Methods in Biomedical Engineering***. 2018;34(5): 18. DOI: 10.1002/cnm.2958.

[55]. Moore, S.M., P.J. McMahon, and R.E. Debski, Bi-directional mechanical properties of the axillary pouch of the glenohumeral capsule: implications for modeling and surgical repair. ***Journal of Biomechanical Engineering***. 2004;126(2): 284-288. DOI: 10.1115/1.1695574.

Fig. 1. Finite element model of the shoulder complex including three bones (in grey), four musculotendinous units (in red), two cartilages (in light blue), and four ligaments (in dark blue) in (a) anterior view, (b) anterior view without subscapularis, (c) posterior view, and (d) posterior view without posterior rotator cuff muscles.

Fig. 2. Three-dimensional motion measurement (left) and relative subject-specific multi-body musculoskeletal model (right). Several most stable markers for each bone segment (i.e., torso, scapula, clavicle, and humerus) were adopted in the multi-body model. The black boxes are surface EMG sensors.

Fig. 3. Deltoid muscle force implementation. See text for details.

Fig. 4. Von Mises stress distribution at 0° (neutral), 10°, 20°, and 30° of abduction in anterior, medial, and posterior views.

Fig. 5. Distribution of the principal stress in the supraspinatus tendon at 30° abduction. Slice views of principal stress in the sagittal plane through the (a) anterior, (b) medial, and (c) posterior section of the supraspinatus tendon. (d) Overview of the supraspinatus and infraspinatus tendons.

Fig. 6. Penetrated views of the Von Mises stress distribution and contact state of the glenohumeral joint at 0°, 10°, 20°, and 30° of abduction.

Fig. 7. Predicted muscle forces of main shoulder muscles at 0°, 10°, 20°, and 30° of abduction in comparison with those in other studies.

Fig. 8. Comparison of (a) the bone-on-bone contact forces and (b) the superior-inferior movement of the humeral centre with respect to the scapula of the simulation results at 0°, 10°, 20°, and 30° of abduction between this study and previous computational and experimental results in the literature.

Table 1 Material properties and element types of the finite element model

Component	Material	Element type	modulus (MPa)	Poisson's ratio (v)	Reference
Bone	rigid	tetrahedral (C3D10)	∞	N/A	[12]
Cartilage	linear elastic	tetrahedral (C3D10)	15	0.45	[11]
Muscle	linear elastic	tetrahedral (C3D10)	168	0.497	[9]
Ligament	hypoelastic	tetrahedral (C3D10)	10.1*	0.4*	[13]

*Baseline modulus and Poisson's ratio determined from a previous measurement. [55]

Table 2 Muscle forces of rotator cuff muscles and deltoid bundles in 0° (neutral), 10°, 20°, and 30° of scapular plane abduction

Muscle	Muscle force in each abduction angle (N)			
	0°	10°	20°	30°
Deltoid anterior	0.75	18.69	30.50	37.88
Deltoid middle	42.73	74.36	90.56	108.40
Deltoid posterior	2.77	0.96	0.91	1.05
Supraspinatus	6.90	12.89	16.86	21.61
Infraspinatus	21.29	44.46	71.75	120.62
Subscapularis	26.21	38.43	46.54	54.23
Teres minor	1.55	0.83	0.86	1.29

Table 3 The results of bone-on-bone contact force, contact area, peak pressure on the glenoid, and the superior-anterior movement of the humeral centre with respect to the glenoid at each abduction angle

Abduction angle	0°	10°	20°	30°
Bone-on-bone contact force (N)	8.18	91.45	146.14	408.07
Contact Area (mm^2)	7.60	31.89	46.13	88.04
Mean pressure on glenoid (MPa)	1.07	2.86	3.17	4.64
Peak pressure on glenoid (MPa)	1.45	4.63	5.19	7.66
Superior-inferior movement of humeral centre (mm)	0	1.43	2.08	1.47

Table 4 Simulated bone-on-bone contact force and its percentage change (%) with respect to the variation of moduli of soft tissues in each abduction angle. Results in brackets represent the percentage change with respect to baseline.

Material	BOBF in N (percentage change % with respect to baseline)								
Muscle	modulus of the muscle in MPa (percentage change w.r.t. baseline)								
	100.8(-40%)	134.4(-20%)	151.2 (-10%)	159.6(-5%)	168(baseline)	176.4(+5%)	184.8(+10%)	201.6(+20%)	235.2(+40%)
0°	30.02(+266.99)	16.7(+104.16)	11.95(+46.09)	10.00(+22.25)	8.18	6.10(-25.43)	5.65(-30.93)	3.92(-52.08)	1.56(-80.93)
10°	138.11(+51.02)	111.90(+22.36)	101.13(+10.59)	96.17(+5.16)	91.45	87.06(-4.8)	83.15(-9.08)	75.41(-17.54)	62.53(-31.62)
20°	233.65(+59.88)	186.04(+27.30)	165.27(+13.09)	155.61(+6.48)	146.14	137.16(-6.14)	128.67(-11.95)	112.98(-22.69)	85.70(-41.36)
30°	492.38(+20.47)	447.90 (+9.59)	427.92 (+4.70)	418.23 (+2.33)	408.70	399.30(-2.30)	390.23(-4.52)	373.32(-8.66)	343.26(-16.01)
Ligament	modulus of the ligament in MPa (percentage change w.r.t. baseline)								
	6.06(-40%)	8.08(-20%)	9.09(-10%)	9.595(-5%)	10.1(baseline)	10.605(+5%)	11.11(+10%)	12.12(+20%)	14.14(+40%)
0°	9.22(+12.71)	8.67(+5.99)	8.44(+3.18)	8.32(+1.71)	8.18	8.11(-0.86)	8.00(-2.20)	7.79(-4.77)	7.39(-9.66)
10°	91.65(+0.22)	91.61(+0.17)	91.55(+0.11)	91.52(+0.08)	91.45	91.45(0.00)	91.41(-0.04)	91.32(-0.14)	91.12(-0.36)
20°	148.16(+1.38)	147.21(+0.73)	146.66(+0.36)	146.38(+0.16)	146.14	145.83(-0.21)	145.56(-0.4)	145.01(-0.77)	143.96(-1.49)
30°	410.84(+0.52)	409.65(+0.23)	409.22(+0.13)	408.94(+0.06)	408.70	408.46(-0.06)	408.20(-0.12)	407.79(-0.22)	406.85(-0.45)
Cartilage	modulus of the cartilage in MPa (percentage change w.r.t. baseline)								
	9(-40%)	12 (-20%)	13.5(-10%)	14.25(-5%)	15(baseline)	15.75(+5%)	16.5(+10%)	18(+20%)	21(+40%)
0°	5.42(-33.74)	6.88(-15.89)	7.58(-7.33)	7.91(-3.3)	8.18	8.55(+4.52)	8.85(+8.19)	9.44(+15.40)	10.56(+29.10)
10°	70.48(-22.93)	82.14(-10.18)	87.09(-4.77)	89.29(-2.36)	91.45	93.53(+2.27)	95.43(+4.35)	99.09(+8.35)	105.60(+15.47)
20°	118.67(-18.80)	134.17(-8.19)	140.50(-3.86)	143.43(-1.85)	146.14	148.69(+1.74)	151.15(+3.43)	155.79(+6.60)	164.07(+12.27)
30°	340.26(-16.75)	385.88(-5.58)	398.05(-2.61)	403.55(-1.26)	408.70	413.58(+1.19)	418.22(+2.33)	426.74(+4.41)	441.19(+7.95)

Table 5 Simulated peak pressure (MPa) on the glenoid and its percentage change (%) with respect to the variation of moduli of soft tissues in each abduction angle. Results in brackets represent the percentage change with respect to baseline.

Material	Peak pressure in MPa (percentage change % with respect to baseline)
Muscle	modulus of the muscle in MPa (percentage change w.r.t. baseline)

	100.8(-40%)	134.4(-20%)	151.2 (-10%)	159.6(-5%)	168(baseline)	176.4(+5%)	184.8(+10%)	201.6(+20%)	235.2(+40%)
0°	3.14(+116.55)	2.17(+49.66)	1.78(+22.76)	1.60(+10.34)	1.45	1.19(-17.93)	1.13(-22.07)	0.86(-40.69)	0.46(-68.28)
10°	5.71(+23.33)	5.16(+11.45)	4.89(+5.62)	4.76(+2.81)	4.63	4.51(-2.59)	4.40(-4.97)	4.17(-9.94)	3.78(-18.36)
20°	6.89(+32.76)	5.94(+14.45)	5.53(+6.55)	5.34(+2.89)	5.19	5.03(-3.08)	4.88(-5.97)	4.58(-11.75)	3.99(-23.12)
30°	8.71(+13.71)	8.22 (+7.31)	7.98 (+4.18)	7.82 (+2.09)	7.66	7.51 (-1.96)	7.35 (-4.05)	7.08 (-7.57)	6.70(-12.53)
Ligament	modulus of the ligament in MPa (percentage change w.r.t. baseline)								
	6.06(-40%)	8.08(-20%)	9.09(-10%)	9.595(-5%)	10.1(baseline)	10.605(+5%)	11.11(+10%)	12.12(+20%)	14.14(+40%)
0°	1.53(+5.52)	1.49(+2.76)	1.47(+1.38)	1.46(+0.69)	1.45	1.43(-1.38)	1.42(-2.07)	1.40(-3.45)	1.37(-5.52)
10°	4.65(+0.43)	4.64(+0.22)	4.64(+0.22)	4.63(0)	4.63	4.63(0)	4.62(-0.22)	4.62(-0.22)	4.61(-0.43)
20°	5.23(+0.77)	5.21(+0.39)	5.20(+0.19)	5.19(0)	5.19	5.18(-0.19)	5.18(-0.19)	5.17(-0.39)	5.15(-0.77)
30°	7.73(+0.91)	7.70 (+0.52)	7.68 (+0.26)	7.67 (+0.13)	7.66	7.66 (0)	7.65 (-0.13)	7.64 (-0.26)	7.61(-0.65)
Cartilage	modulus of the cartilage in MPa (percentage change w.r.t. baseline)								
	9(-40%)	12 (-20%)	13.5(-10%)	14.25(-5%)	15(baseline)	15.75(+5%)	16.5(+10%)	18(+20%)	21(+40%)
0°	0.918(-36.69)	1.19(-17.93)	1.32(-8.97)	1.38(-4.83)	1.45	1.51(+4.14)	1.57(+8.28)	1.69(+16.55)	1.93(+33.10)
10°	3.17(-31.53)	3.94(-14.90)	4.29(-7.34)	4.46(-3.67)	4.63	4.80(+3.67)	4.96(+7.13)	5.27(+13.82)	5.86(+26.57)
20°	3.65(-29.67)	4.46(-14.07)	4.84(-6.74)	5.01(-3.47)	5.19	5.36(+3.28)	5.53(+6.55)	5.85(+12.72)	6.45(+24.28)
30°	5.58(27.15)	6.69(-12.66)	7.19(-6.14)	7.43(-3.00)	7.66	7.90(+3.13)	8.12(+6.01)	8.55(+11.62)	9.38(+22.45)

General Response

We thank both reviewers for their positive comments and constructive suggestions. We respond to the individual points in detail below, indicating the corresponding changes that we have made within the manuscript.

Specific Responses to Reviewer #1

The authors adequately responded to my previous comments and made according changes in the paper. However, I would like to join the first reviewer in the request to carefully consider the style and English grammar of the paper once again. The Discussion section needs special attention. I attach some suggestions for the first two pages of it here.

Author Response: As suggested, we have further thoroughly revised the manuscript with special attention to the Discussion section.

Specific Responses to Reviewer #2

The text is now more readable but your editorial service do not seem to understand the text and I suggest that in the minor further revision which is required you run it past a native English speaking engineer. I have made suggestions for improving the English, as well as asking some questions where clarifications are required, all on the attached annotated manuscript.

Author Response: As suggested, we have further thoroughly revised the manuscript with the help of a native English speaking engineer.

"Also, the surface area of the glenoid cartilages (without labrum) was found to be 416 mm2." This is a weakness. the labrum is very much a functional part of the joint in controlling motion, and probably transferring forcrs an should be taken into consideration

Author Response: Indeed, the omission of the labrum is a limitation of this study. This was mentioned in the Discussion section in Page 9 line 10 as "It should be noted that the labrum was not included in this study, which may had resulted in an underestimated contact area. Future work in this study will focus on integrating the labrum-biceps complex into the model to enable the model to investigate more complex shoulder biomechanical conditions."

"During the rotation and translation, all rotator cuff muscles were manually 17 pre-stressed to avoid compression occurred in any portion of the muscles and tendon." how? and how does this avoid compression? and should be 'compression occurring'

Author Response: The expression was revised to "compression occurring" as suggested. The occurring of the compression can be checked in the simulation results. By examining the results of the geometries acquisition simulations, no compression occurred in any portion of the muscles and tendon.

Figure 1

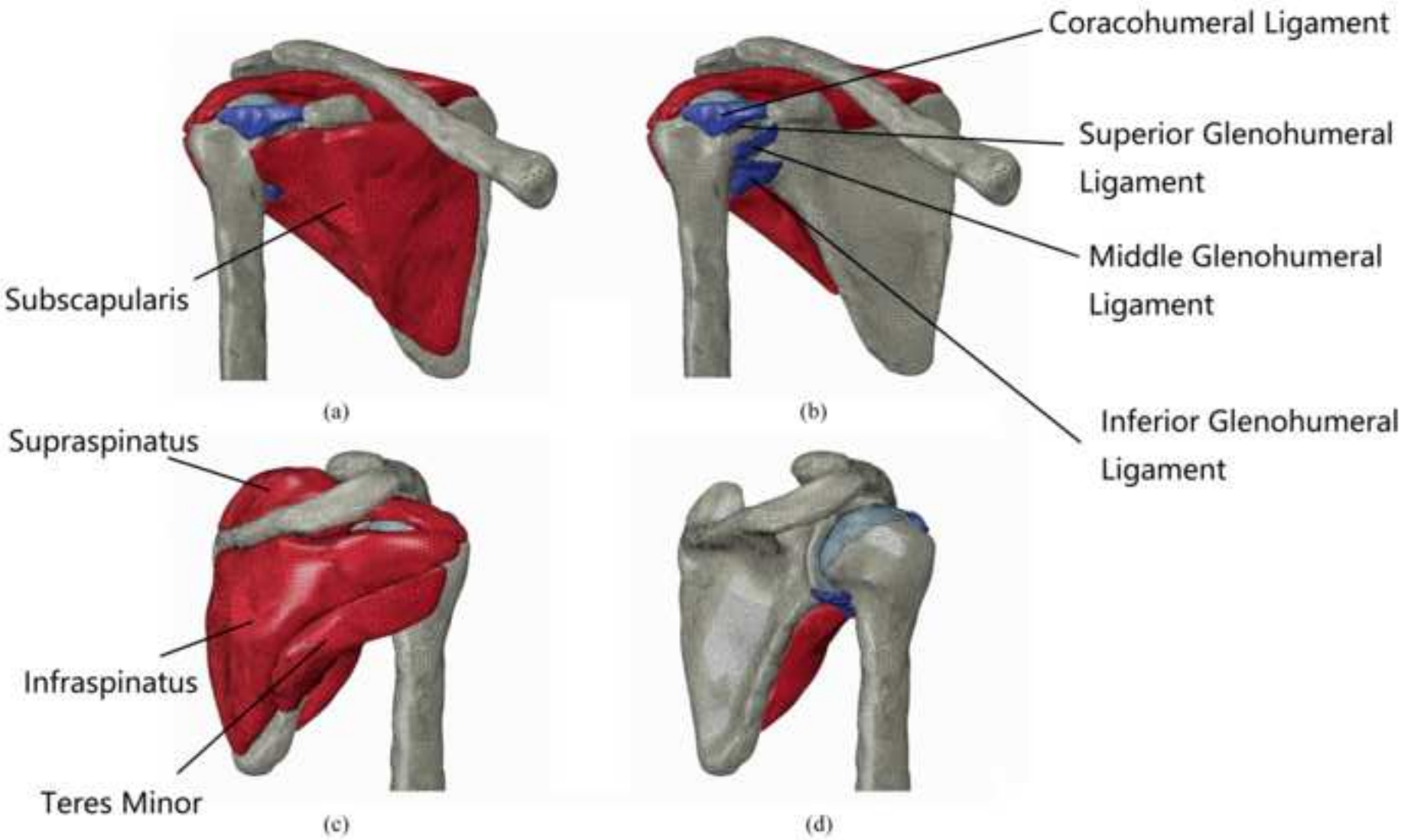

Figure 6

Click here to access/download;Figure;Zheng,6.tif

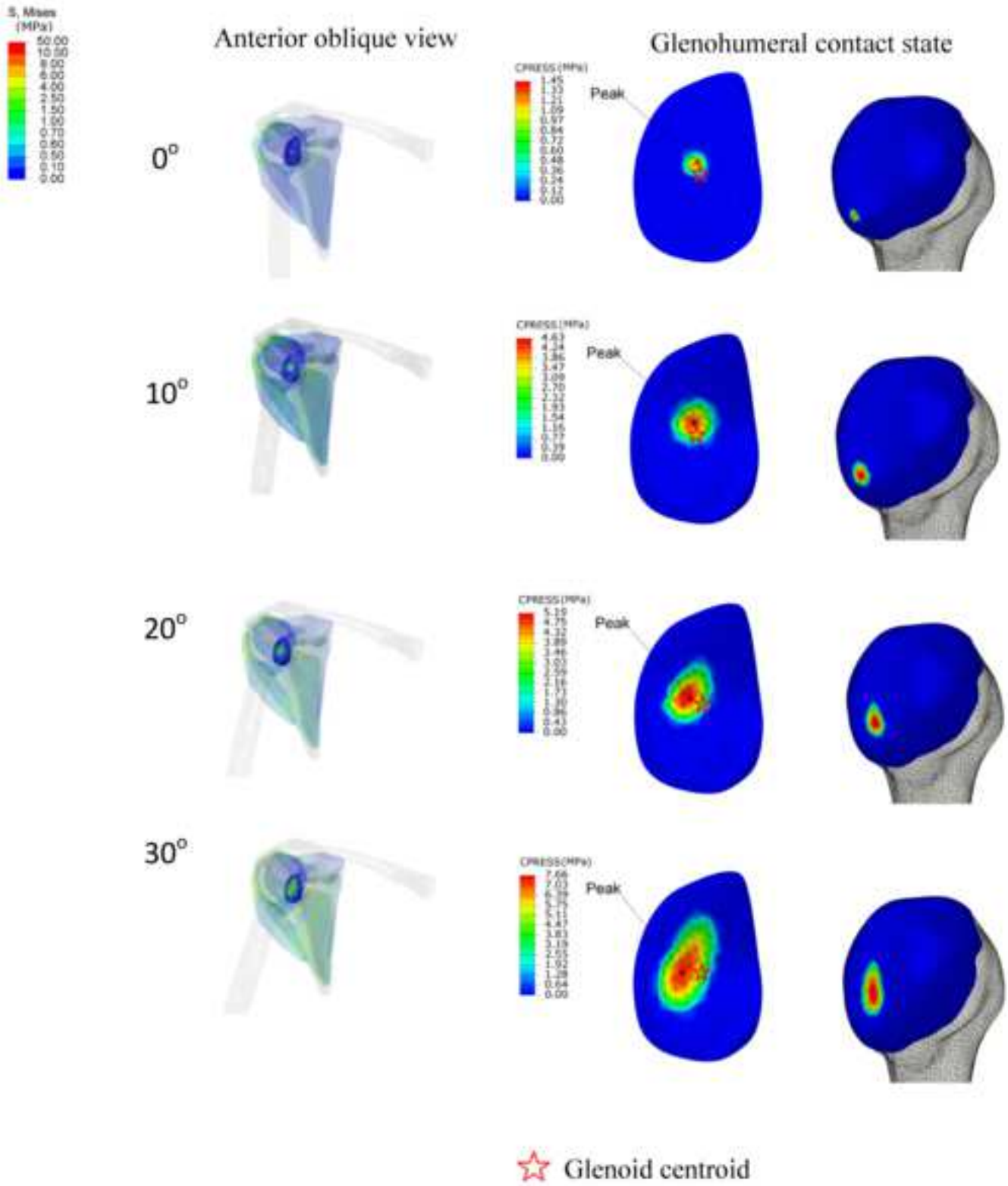

Figure 2

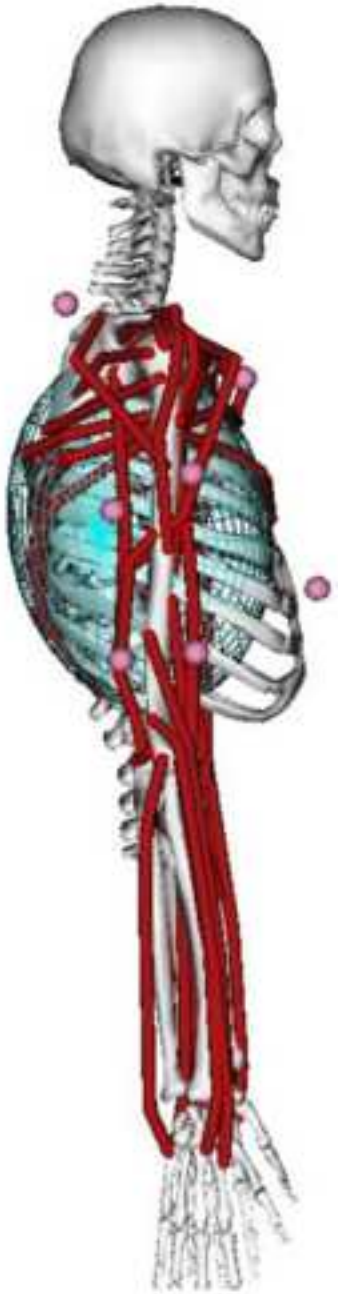

Figure 3

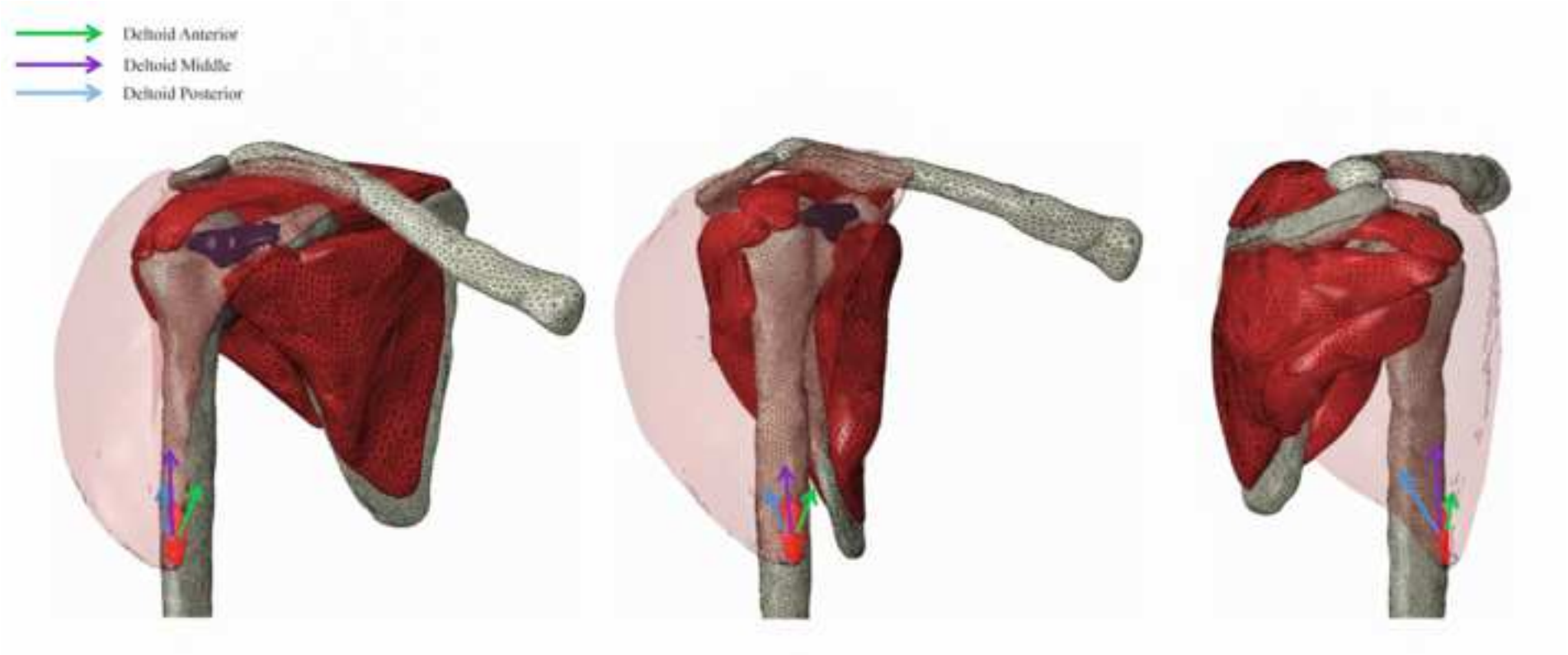

Figure 4

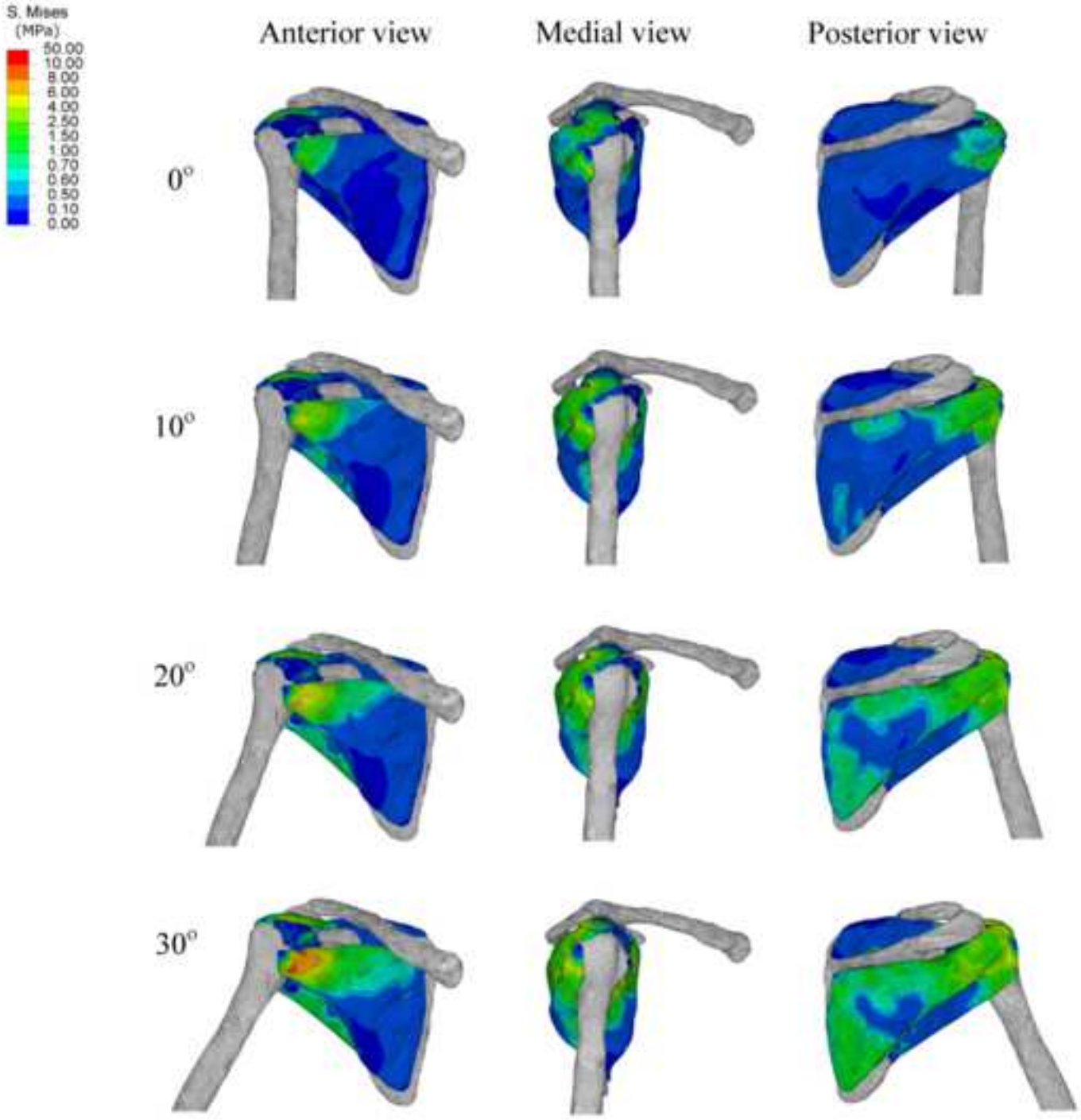

Figure 5

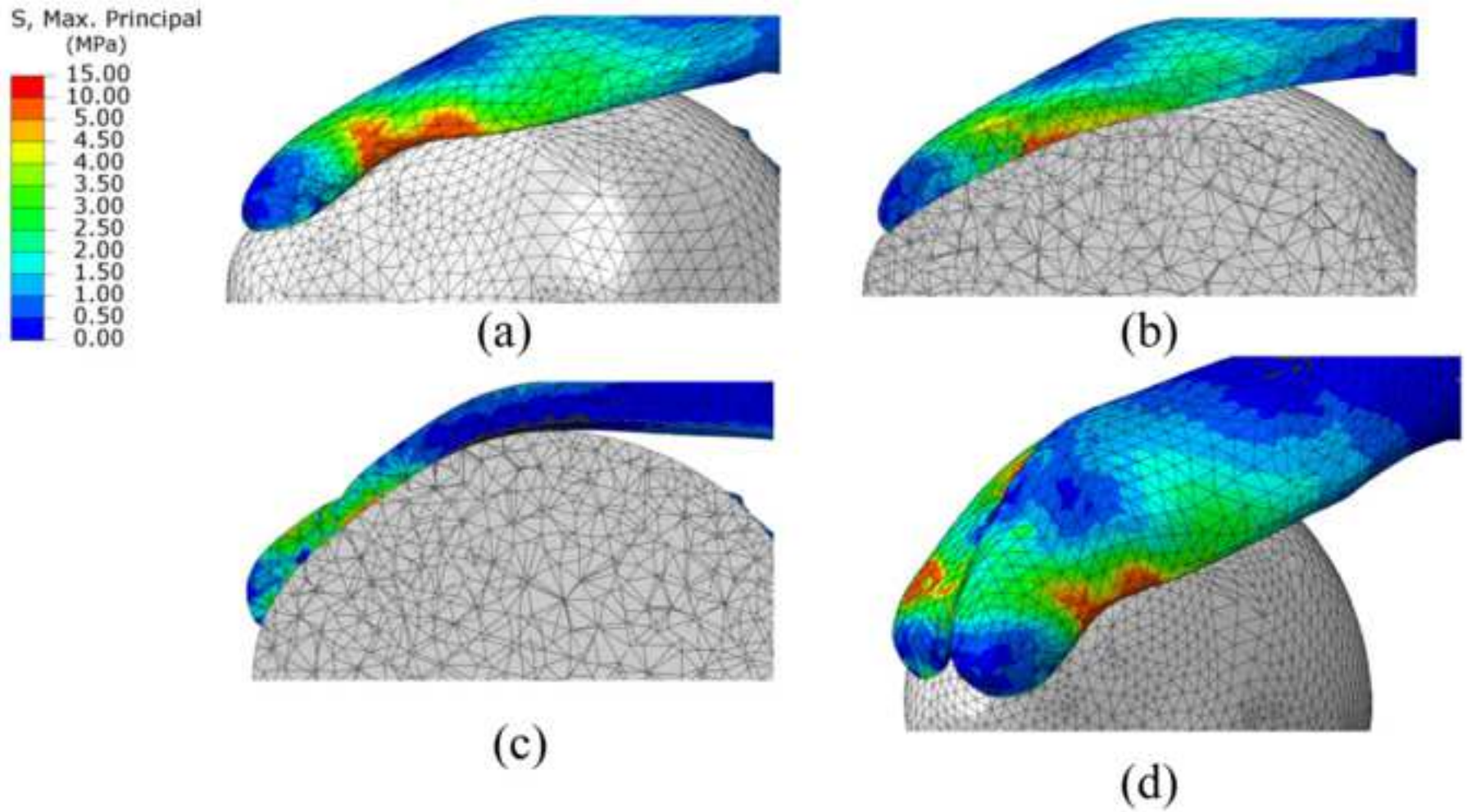

Supplement

Figure 7


Click here to access/download
Supplementary Material
Zheng,7.emf

Figure 8


Click here to access/download
Supplementary Material
Zheng,8.emf